Published in Proceedings of The 25th Army Science Conference (2006).

TAILORING OF NANO- AND MICROSTRUCTURE IN BIOMIMETICALLY SYNTHESIZED CERAMIC FILMS

Guangneng Zhang and Junghyun Cho*
Dept. of Mechanical Engineering & Program of Materials Science and Engineering
State University of New York at Binghamton
Binghamton, NY 13902-6000

ABSTRACT

A novel ceramic thin film deposition approach through which inorganic materials were deposited on a functionalized organic matrix from aqueous media at low temperatures was studied. This process is analogous to the natural biomineralization process. Specifically, nanostructured ZrO_2 and TiO_2 thin films were deposited at about 70°C by the hydrolysis of $Zr(SO_4)_2$ and $TiCl_4$ aqueous precursor solutions, respectively, on silicon substrates coated with phosphonate-terminated self-assembled monolayers (SAMs). The as-deposited oxide films consisted of nanocrystallites of tetragonal ZrO_2 and anatase phase TiO_2 in size of 5-10 nm, while some amorphous phases existed as well. The principal mechanism for the formation of the films seems to be homogeneous nucleation of the bulk precipitates and their aggregation behavior in supersaturated solution. Different from the previous results, the ZrO_2 and TiO_2 films could also be deposited on bare silicon substrates without any SAMs, under the same conditions used for deposition on SAMs.

The Derjaguin, Landau, Verwey and Overbeek (DLVO) theory was applied to disclose the mechanisms for the formation of the oxide films in the media of aqueous precursor solutions. The interactions of particle-substrate, particle-deposited film, and particle-particle all exhibit negative minimal energies, indicating that the initial and subsequent continuous depositions on SAM and bare silicon, as well as particle aggregation, are thermodynamically favorable. In addition, the differences among the amplitudes of the minimal interaction energies may, however, reflect some preference of the deposition on SAMs to that on bare silicon.

In an effort to evaluate mechanical integrity of the as-deposited ceramic films, the intrinsic elastic moduli of the as-deposited ceramic films were determined by using dynamic nanoindentations. Dye leak tests suggest that the as-deposited ceramic films, especially the TiO_2 films, enhance significantly the hermeticity performance of the device coatings.

1. INTRODUCTION

Ceramics have provided a powerful driving force for realization of many advanced technologies due to their excellent structural and functional properties. In particular, ceramic thin films have found applications in fuel cells, semiconductors, electronic packaging, optical equipment, thermal barrier coatings, and wear-resistant coatings. In addition, ceramic films have shown a potential for protective coatings for MEMS and harsh-environment electronic devices (Rajan et al., 1998). Importantly, ceramic coatings and films would benefit the MEMS packaging by relaxing the stringent requirements for the assembly (Maluf 2000), thereby drastically reducing the packaging cost.

Numerous deposition techniques have been applied to synthesize ceramic thin films. These techniques fall into at least two categories: 1) vacuum-based methods such as chemical vapor deposition, physical vapor deposition, and 2) solution-based methods including sol-gel, electrochemical deposition, and hydrothermal synthesis (Gao et al., 2005). Vacuum-based techniques require an expensive investment, are limited to line-of-sight production (especially for physical vapor deposition), and usually require high-vapor-pressure chemicals or high-purity targets as starting materials. On the other hand, solution-based methods mentioned above can overcome some of the obstacles of vacuum-based methods by use of a homogeneous solution, but there are still some processing issues, such as the control of the film thickness at the nanometer scale of length and complex processing control (Gao et al., 2005).

Novel techniques for the synthesis of ceramic films from aqueous solutions at low temperatures are emerging as promising alternatives to traditional vapor-phase and solution-based techniques. The main techniques, including chemical bath deposition, liquid phase deposition methods, and electroless deposition, along with their variations, were summarized in recently published review articles (Niesen et al., 2001; Gao et al., 2005).

Interestingly, the best example of controlled synthesis of inorganic material structures is often observed in nature. In biological environments, biomineralization, such as the formation of eggshells, teeth, and bones, involves the controlled nucleation and growth of inorganic materials from aqueous solutions. Biomineralization can be implemented in four basic steps (Mann 2001): 1) supramolecular pre-organization via construction of an organized reaction environment; 2) interfacial molecular recognition, where the organic supramolecular systems provide a framework for the assembly of the inorganic phase; 3) assembly of the mineral phase through crystal growth and termination enabling the formation of textures and shapes; and 4)

formation of higher order architectures. Hence, an essence of biomineralization is that it is regulated by the organic matrix that works as either compartments for mineralization, heterogeneous nucleation sites, substrates for specific crystallization, or scaffolds that define macroscopic shapes (Schmid 1998).

In recent years, the principle of the biomineralization has been employed in the deposition of inorganic thin films using self-assembled monolayers (SAMs) with specific surface functionalities as organic templates (Shin et al., 1995; Agarwal et al., 1997; Zhang et al., 2006). SAMs have long been popular as templating agents due to their tailored surface properties. SAMs are highly ordered and oriented molecular assemblies usually formed by the chemical absorption of an active surfactant on a solid surface. A general molecular formula of a common species of SAMs, typically formed by hydrolysis-condensation reactions, is $RSiX_3$, where "R" is an organic functional group and "X" is an alkoxide or halide. According to the biomimetic concept, the ionized surface functional groups of SAMs can facilitate or mediate the deposition of inorganic materials if substrates containing such SAMs are in contact with appropriate solutions containing suitable precursors. In recent years, this approach has been applied to the deposition of a variety of inorganic materials including TiO_2, Y_2O_3/ZrO_2, FeO(OH), V_2O_5, $SrTiO_3$, ZnO, SnO_2, $CaCO_3$, ZnS, and PbS, as summarized in Ref. (Gao et al., 2005). More importantly, this deposition process is usually accomplished under mild conditions in terms of low temperature (usually <100°C) and normal pressure and atmosphere. This approach is an attractive alternative for the preparation of inorganic thin films, especially in applications in which the substrate cannot be exposed to high temperatures or for energy-efficient processes.

Our previous research (Yang et al., 2004; Zhang et al., 2005 and 2006) focused on the synthesis of ZrO_2 thin films deposited on a SAM-coated silicon substrate from a precursor solution at near room temperatures. Recently, we succeeded in the synthesis of TiO_2 thin films with the similar method. The mechanisms responsible for ceramic deposition, based on the DLVO theory, were systematically explored at various processing conditions. One purpose here is to discover the fundamental relationships that link kinetic control of nucleation and growth of the nanoparticles to nano- and microstructure evolution of the oxide films. This study is supplemented with extensive HR-TEM and SEM characterizations for monitoring structural evolution, with nanoindentation for assessing mechanical performance, and with dye leak testing for hermeticity evaluation.

2. EXPERIMENTS

2.1 SAM deposition on silicon

The silicon substrates used in this study were n-type (100) single crystal silicon wafers (Silicon Quest International, Santa Clara, CA) and parylene thin film coated on the silicon wafers mentioned above. The silicon wafers were cut into ca. 13mm x 14mm samples. The silicon substrates were then sonicated in acetone, and then cleaned by freshly prepared piranha solution (1 part 30% H_2O_2 + 3 parts 98% H_2SO_4) for 30 min to obtain a hydrophilic surface. The SAMs were then deposited on the hydrolyzed silicon substrates by immersion in a 1 vol% diethylphosphatoethyltriethoxysilane ($C_{12}H_{29}O_6PSi$; Gelest Inc., Morrisville, PA) anhydrous acetonitrile solution for 12 h inside a nitrogen-filled glovebox where moisture concentration was maintained at ca. 1 ppm at room temperature. The SAM-coated substrates were then sonicated with ethanol and dried completely with nitrogen gas. The SAMs were further hydrolyzed by immersing the substrates in 1 M HCl solution at 70˚C in order to obtain a suitable surface terminus ($-PO(OH)_2$) for the subsequent ZrO_2 and TiO_2 depositions.

2.2 Deposition of ZrO_2 films

The deposition of ZrO_2 films was carried out through a near-room temperature aqueous solution process. A freshly prepared 1 mM zirconium sulfate ($Zr(SO_4)_2 \cdot 4H_2O$, 99.99%, Alfa Aesar, Ward Hill, MA) + 0.2 M HCl aqueous solution was used as precursor solution. Appropriate amount of concentrated HCl was first added into de-ionized water and then the zirconium sulfate was added into the HCl solution. The order of adding the reagents was important in that it avoided the possibility of extensive hydrolysis of the zirconium sulfate at higher pH condition. The pH of the precursor solution was ca. 0.88.

The SAM-coated substrates were placed upside-down on the ceiling of a horizontally-positioned parallel plate channel through which the precursor solution would flow. The height of the channel was ca. 1 mm. The deposition setup was kept in a constant temperature bath set at 70°C. A stepwise deposition process was implemented by changing the precursor solution with the freshly prepared one every 2 h. After 1 to 4 deposition steps and correspondingly deposition time of 2 to 8 h were reached, the substrates were taken out from the deposition setup and rinsed and sonicated with anhydrous ethanol for 10 min, and then dried completely with nitrogen gas. Clean and hydrolyzed bare silicon substrates with no SAM were used as controls for all experiments.

2.3 Deposition of TiO_2 films

The deposition of TiO_2 films followed the same paradigm used for ZrO_2 deposition. A freshly prepared titanium chloride ($TiCl_4$, 99.999%, Alfa Aesar, Ward Hill, MA) + 0.05 M HCl aqueous solution was used as precursor solution. The titanium chloride was used as it was from the manufacturer without any further purification. Due to the extreme reactivity of $TiCl_4$, efforts were made to reduce the loss of $TiCl_4$ during the preparation of precursor solution. The $TiCl_4$ was added

slowly with magnetic stirring into 0.05 M HCl aqueous solution which was cooled in an ice-water bath. Even under the low temperature condition, however, there was still a vigorous and exothermic reaction along with generation of white fume of HCl droplets. The concentration of titanium (IV) ions in the titanium chloride precursor solution was later determined to be 8.8 mM by using inductively coupled plasma (ICP) analysis, indicating a lost of $TiCl_4$ of ca. 12% during the preparation. The pH of the precursor solution was ca. 1.32.

The SAM-coated substrates were placed upside-down on the ceiling of the horizontally-positioned parallel plate channel as mentioned above. The deposition setup was kept in a constant temperature bath set at 70°C. After 1 to 4 deposition steps and correspondingly deposition time of 2 to 8 h were reached, the substrates were taken out from the deposition setup and rinsed and sonicated with anhydrous ethanol for 10 min, and then dried completely with nitrogen gas. Clean and hydrolyzed bare silicon substrates with no SAM were also used as controls.

2.4 Characterizations of solutions and ceramic films

The size of the ZrO_2 and TiO_2 precipitates in the precursor solutions, particularly at the early stages of precipitation, was studied with dynamic light scattering (DLS) (Zetasizer Nano S, Malvern Instrument, UK).

The nanostructure of the as-deposited ZrO_2 and TiO_2 films were characterized by using a high-resolution field emission gun transmission electron microscope (TEM, HF-2000, Hitachi). Evolution of film morphology was examined using scanning electron microscope and optical microscope. Mechanical properties of the as-deposited films were characterized using nanoindentation (TriboIndenter®, Hysitron Inc., Minneapolis, MN). Penetrant dye gross leak tests were employed to characterize the hermeticity of the ceramic thin films.

3. FORMATION OF CERAMIC FILMS

Generally, the ceramic film formation can be achieved through two nucleation mechanisms (Zhang et al., 2005): 1) heterogeneous nucleation at the interface between the substrate and solution, and 2) homogeneous nucleation by forming stable nuclei in a supersaturated solution. In the former mechanism, dissolved ionic species may attach to the SAM surface through an ion-by-ion growth mechanism. This is connected to directed growth of nuclei of the inorganic phase and formation of crystalline structures. However, little evidence of the former mechanism has been found for the deposition of ZrO_2 and TiO_2 films in our study. In the latter mechanism, ZrO_2 and TiO_2 nuclei formed by homogeneous nucleation can grow into colloidal particles in solution and be attracted to the properly treated surface as a result of electrostatic and/or van der Waals interactions.

Our previous studies (Zhang et al., 2005; Zhang et al., 2006) demonstrated that the as-deposited ZrO_2 films consist of tetragonal ZrO_2 crystallites in size of 5-10 nm, as shown in Fig. 1. The cross-sectional TEM analysis also suggested that there was a random orientation of the ZrO_2 crystallites near the ZrO_2/SAM-SiO_2 interface and across the film thickness direction. This random orientation of the crystallites indicated the dependence on the homogeneous nucleation mechanism. It should be noted that the cross-sectioned specimens were not thin enough to have a single layer of ZrO_2 crystallites for the determination of unambiguous crystal orientation; in fact, the cross-sectional TEM images reflected the overlapping of a few layers of the ZrO_2 crystallites. Energy dispersive X-ray spectroscopy (EDS) analysis on the as-deposited ZrO_2 films revealed small amounts of sulfur (S), believed to be from the remaining amorphous $Zr(SO_4)_2$ that did not transform to ZrO_2 under the reaction regime proposed in other studies (e.g., Agarwal et al., 1997).

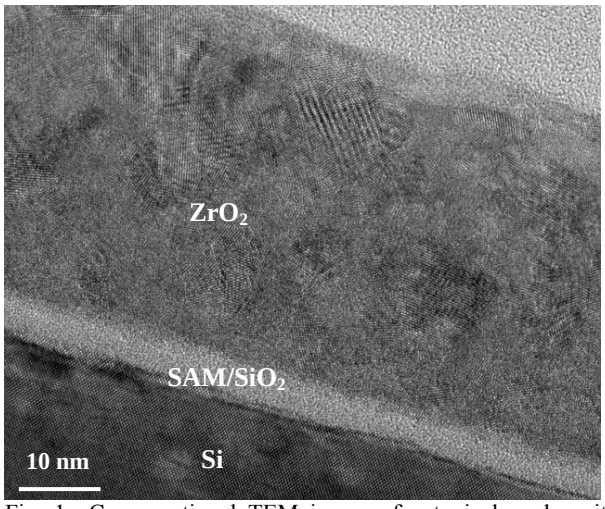

Fig. 1 Cross-sectional TEM image of a typical as-deposited ZrO_2 film on a SAM-coated silicon substrate.

One example of nanostructure developments of a ZrO_2 film is shown in Fig. 2. Nanocrystallites of 5-10 nm in size are initially formed on the SAM-coated substrate (Fig. 2 (a)). These initial crystal sizes are consistent with the results from the DLS measurements on initial precursor solutions. Once they are formed at the substrate surface, these crystals attract more nanocrystals around them resulting in the formation of isolated islands of 50-100 nm in size. As they continue to grow laterally, the island structures become connected (Fig. 2 (b)), and finally form a continuous film (Fig. 2 (c) and (d)).

The as-deposited TiO_2 films showed similar nanostructures with those of ZrO_2 films in terms of size and orientation of the crystallites. Typical cross-sectional nanostructures of the as-deposited TiO_2 films on SAM-coated silicon substrates at 70˚C for 8 h are shown in Fig. 3. The films consist of anatase TiO_2 nanocrystallites as indicated by electron diffraction (inset, Fig. 3). The observed d-spacings from the diffraction patterns

indicated d_{101} = 3.487 Å, d_{200}=1.900 Å, d_{004} = 2.394 Å, and d_{105}=1.704 Å which are very close to those of anatase. The diffuse ring in the diffraction pattern indicated some amount of amorphous phase in the TiO_2 films. The size of the TiO_2 crystallites is in the range of 5-10 nm, which is consistent with the size of the TiO_2 particles obtained from the used precursor solution, as shown in Fig. 4. The orientations of the TiO_2 crystallites seem to be random as is those of the ZrO_2 crystallites. EDS analysis showed little amount of chlorine, suggesting the absence of remaining $TiCl_4$ in the films. The as-deposited TiO_2 films showed different morphology (Fig. 5) to that of ZrO_2 films, in that the TiO_2 films were more rugged and particulate while the ZrO_2 films exhibited rounded island structure and looked much smoother. The TiO_2 films exhibited less likely occurrence of crack than did the ZrO_2 films.

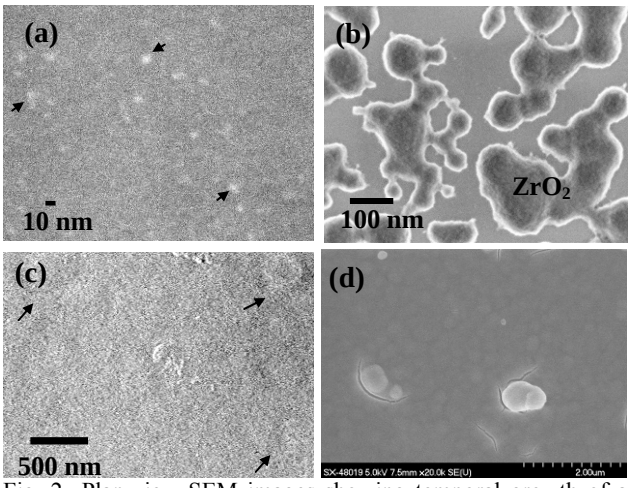

Fig. 2 Plan-view SEM images showing temporal growth of a ZrO_2 film on SAM-coated silicon: (a) nanocrystallites (5-10 nm in size) at a very early stage (arrows); (b) island structures made of nanocrystallites at an intermediate stage; (c) continuous films formed at the final stage (8 h of deposition); (d) cracks in the films were formed possibly due to embedment of large aggregates and/or incompatible drying process.

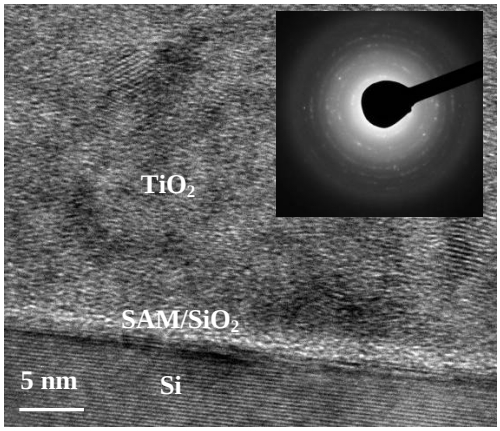

Fig. 3 Cross-sectional TEM image of a typical as-deposited TiO_2 film on a SAM-coated silicon substrate. Inset: electron diffraction pattern of the TiO_2 crystallites.

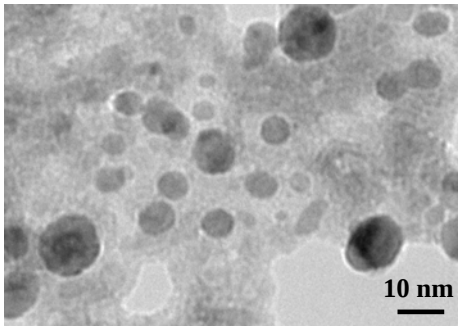

Fig. 4 TEM image of TiO_2 particles obtained from the 8.8 mM $TiCl_4$+0.05 M HCl precursor solution after being heated at 70℃ for 2 h.

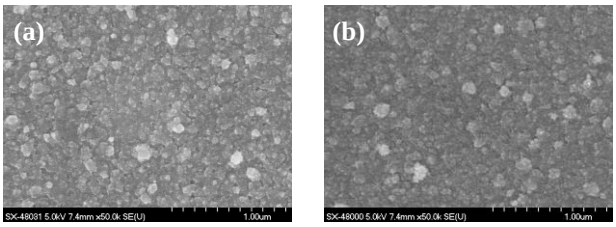

Fig. 5 SEM images of the as-deposited TiO_2 films (plan-view) on SAM-coated silicon substrates. Deposition conditions are 8.8 mM $TiCl_4$ + 0.05 M HCl precursor solution, 70℃, and (a) 4 h (2 steps), (b) 8 h (4 steps).

The dynamic light scattering (DLS) analysis provided an alternative view of the kinetics of particle growth and aggregation which is crucial to the ceramic deposition. The DLS results indicated that both the ZrO_2 and TiO_2 grow from particles of 5-10 nm in size in the very initial stage, as also revealed by the TEM analysis. As the growth continues, aggregation between particles occurs, and the ZrO_2 and TiO_2 start to display distinct aggregation behaviors as shown in Fig. 6, in that the ZrO_2 aggregates to above 600 nm in size in about 20 min, while the TiO_2 aggregates to about 45 nm and maintained that size for a longer time period. The difference in the size of aggregates for ZrO_2 and TiO_2 may explain the difference in the morphologies of the two films as discussed above.

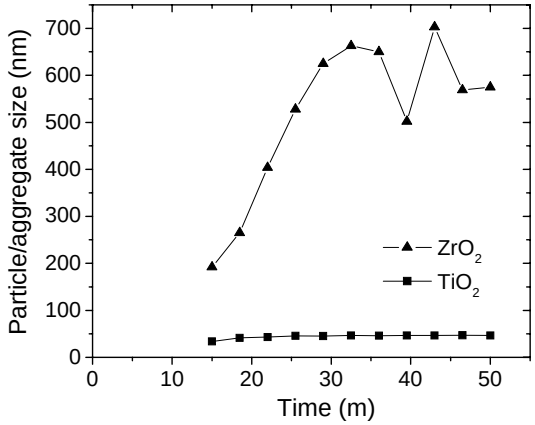

Fig. 6 Particle growth and aggregation of ZrO_2 and TiO_2 in the precursor solutions at 70℃ as measured by DLS.

Surprisingly, we found that ZrO_2 and TiO_2 films can also be deposited on the cleaned and hydrolyzed bare silicon substrates without any SAM anchored, under the same deposition condition as those used in SAM coated silicon substrates, as described in Section 2. Previous references (e.g., Agarwal et al., 1997; Shin et al., 1998; Zhang et al., 2006) have reported that ZrO_2 films cannot be deposited on bare silicon substrates under their specific deposition conditions. This discrepancy may arise from the different deposition conditions. Specifically, the precursor solutions we used had a much lower species concentration than those reported in the references.

The morphology and nanostructures of the TiO_2 films deposited on bare silicon substrates showed little significant difference with those deposited on SAM-coated silicon substrates. The films deposited on bare silicon substrates displayed enough adhesion with the substrates, in that they survived after being sonicated in ethanol for 10 min. However, the two TiO_2 films demonstrated some difference in growth kinetics, specifically at the initial 4 h. Fig. 7 (a) and (b) show the TiO_2 film deposited on a bare silicon substrate without any SAM coating, from a 8.8 mM $TiCl_4$ + 0.05 M HCl precursor solution in 70℃, for 4 h (2 steps, each 2 h) and 8 h (4 steps, each 2 h), respectively. The significant difference between Fig. 5 (a) and Fig. 7 (a) suggests that the TiO_2 film grown on SAM yields higher deposition rate than that grown on bare silicon at the initial 4 h. Virtually no continuous film was formed on bare silicon within the initial 4 h. During the subsequent deposition, the two films showed similar deposition rate, both forming continuous film, as suggested by the similarity between Fig. 5 (b) and Fig. 7 (b). The ZrO_2 films deposited on bare silicon substrates also showed similar behaviors as the TiO_2 films. The driving forces for deposition of the ceramic films on SAM and bare silicon will be elaborated with DLVO theory in the Section 4.

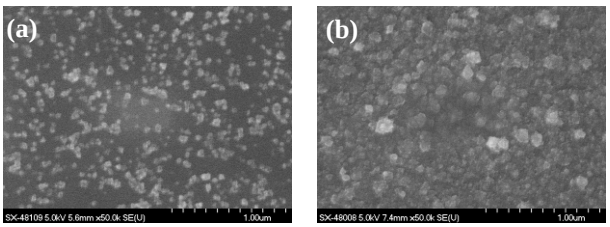

Fig. 7 SEM images of the as-deposited TiO_2 films (plan-view) on bare silicon substrates. Deposition conditions are (a) 8.8 mM $TiCl_4$ + 0.05 M HCl precursor solution, 70℃, 4 h (2 steps, each 2 h). (b) 8.8 mM $TiCl_4$ + 0.05 M HCl precursor solution, 70℃, 8 h (4 steps, each 2 h).

4. APPLICATION OF DLVO THEORY

The Derjaguin, Landau, Verwey and Overbeek (DLVO) theory describes the force between surfaces interacting through a liquid medium. It originally combines the electrostatic interaction due to the electric double-layer and the van der Waals interaction which arises from the polarization of molecules into dipoles. In an "extended" DLVO theory (Hogg et al., 1966), the repulsive interaction in very short distances (<2 nm) between hydrophilic surfaces on which water molecules are bound is also included.

According to the "extended" DLVO theory, the total interaction energy (V_{tot}) between the substrate (with subscript 1) and particle (with subscript 2) is the addition of three parts as:

$$V_{tot} = V_e + V_a + V_r \qquad \text{Eq. 1}$$

where V_e is the energy associated with the electrostatic interaction, V_a is the energy associated the London-van der Waals interaction, and V_r is the energy associated the short-range repulsion due to the hydration potential.

The electrostatic interaction between a flat and infinitely large surface and a spherical particle in a medium can be rewritten as (Hogg et al., 1966):

$$V_e = \varepsilon_0\varepsilon_3\pi R\left[\left(\psi_1+\psi_2\right)^2\ln\left(1+e^{-\kappa x}\right)+\left(\psi_1-\psi_2\right)^2\ln\left(1-e^{-\kappa x}\right)\right] \qquad \text{Eq. 2}$$

where R is the radius of particle, x is the separation between the two concerned objects, ε is the dielectric constant, the subscripts 1, 2, and 3 stand for the substrate, the particle, and the medium, respectively, ε_0 is the permittivity of free space, and κ is the reciprocal of the Debye length which is determined as (Israelachvili 1985):

$$\kappa^{-1} = \sqrt{\frac{\varepsilon_0\varepsilon_3 k_B T}{q_e^{\,2}\sum_i N_i Z_i^{\,2}}} \qquad \text{Eq. 3}$$

where k_B is the Boltzmann's constant, q_e is the charge of electron, T is the absolute temperature in Kelvin, N_i is the number of ion i in unit volume of the medium, and Z_i is the valence of ion i.

For interaction between a spherical particle (subscript 2) with another like spherical particle (subscript 2) with the same radius R in a medium (subscript 3), the Eq. 2 can be rewritten as:

$$V_e = 2\varepsilon_0\varepsilon_3\pi R\psi_2^{\,2}\ln\left(1+e^{-\kappa x}\right) \qquad \text{Eq. 4}$$

The van der Waals interaction arises from the normally attractive force between transient dipoles in molecules without permanent multipole moments. The van der Waals interaction energy between a flat and infinitely large substrate (1) and a spherical particle (2) in a medium (3) is determined as

$$V_a = -\frac{A_{132}}{6}\left[\frac{2R(R+x)}{x(x+2R)}-\ln\left(\frac{x+2R}{x}\right)\right] \qquad \text{Eq. 5}$$

where the Hamaker constant (A) for a flat and infinitely large substrate (subscript 1) and a spherical particle (subscript 2) can be determined using the Lifshitz method as (Ackler et al., 1996):

$$A_{132} = \frac{3}{4}k_B T\left(\frac{\varepsilon_1-\varepsilon_3}{\varepsilon_1+\varepsilon_3}\right)\left(\frac{\varepsilon_2-\varepsilon_3}{\varepsilon_2+\varepsilon_3}\right)+ \frac{3h\nu_e}{8\sqrt{2}}\frac{(n_1^{\,2}-n_3^{\,2})(n_2^{\,2}-n_3^{\,2})}{\sqrt{n_1^{\,2}+n_3^{\,2}}\sqrt{n_2^{\,2}+n_3^{\,2}}\left(\sqrt{n_1^{\,2}+n_3^{\,2}}+\sqrt{n_2^{\,2}+n_3^{\,2}}\right)} \qquad \text{Eq. 6}$$

The van der Waals interaction energy between a spherical particle (subscript 2) and another like particle (subscript 2) with the same radius R in a medium (subscript 3) is determined as (Israelachvili 1985):

$$V_a = -\frac{A_{232}R}{12x} \quad \text{Eq. 7}$$

where the Hamaker constant for two like spherical particle (2) in a medium (3) can be determined as:

$$A_{232} = \frac{3}{4}k_BT\left(\frac{\varepsilon_2-\varepsilon_3}{\varepsilon_2+\varepsilon_3}\right)^2 + \frac{3h\nu_e}{16\sqrt{2}}\frac{(n_2^2-n_3^2)^2}{\left(n_2^2+n_3^2\right)^{3/2}} \quad \text{Eq. 8}$$

The repulsive energy associated with hydration interaction can be evaluated as (Kallay et al., 1987):

$$V_r = \frac{As^6}{7560}\left[\frac{8R+x}{(2R+x)^7}+\frac{6R-x}{x^7}\right] \quad \text{Eq. 9}$$

where s (= 0.5×10^{-9} m) is the collision diameter of the oxide particles (Shin et al., 1998).

Despite these analytical equations, for at least a couple of reasons, the use of the DLVO theory in this study must be considered approximate and the values of the interaction energies thus obtained can be meaningful only when they are used to demonstrate the trends regarding different conditions. First, many of the relevant parameters in the calculations are not known precisely or can only be estimated, such as the zeta potential of SAM at various pH conditions and the index of refraction of the SAM. Second, some of the important parameters in the calculations, such as radius of particles, concentration of species in the solution, and mean separation of the particles, change with time during deposition.

The DLVO interaction during ceramic deposition process can be considered with different time frames. At the initial stage when there is little ceramic material deposited on the surface of the substrate, the major interaction contributed to deposition is the interaction between the particle and the substrate (V_{ps}) in the precursor solution. The surface can be SAM coated or non-coated, which could result in different interaction behaviors. As deposition goes on, the substrate would be covered with a few monolayers of the ceramic materials, and the major interaction contributed to deposition changes to be the interaction between the particle and the deposited film (V_{pf}). In addition to the interaction contributing to deposition, the interactions between like particles (V_{pp}) in the precursor solution should also be considered in that they control the undesired aggregation of the particles.

The materials properties involved in the DLVO calculations in this study are listed in Table 1. The optical properties of the phosphonate SAM used in this study were reasonably estimated based on literatures (Israelachvili 1985; Shin et al., 1998).

The deposition conditions involved in the DLVO calculations are listed in Table 2. These conditions, except the radius of particles and concentrations of electrolyte, are equal to those used in actual depositions. The radius of particles was considered to be 5 nm based on the TEM and DLS analysis. The electrolyte refers to the residual alkaline ions whose concentration has an effect on the Debye length of the electric double layers and has been estimated to be 1×10^{-7}M based on the purity of the precursor species.

Table 1 Materials properties included in the DLVO calculations. Values with asterisk (*) are estimated.

Materials	Dielectric constant (at 1 MHz)	Index of refraction (at 70℃)	Isoelectric point	Zeta potential at pH 1
ZrO_2	12.5	2.157	3.5	32 mV
TiO_2	86	2.605	6.05	36 mV
SiO_2/Si	4.42	1.459	3	28 mV
SAM	3*	1.720*	2*	20* mV

Table 2 Deposition conditions included in the DLVO calculations.

	Deposition of ZrO_2	Deposition of TiO_2
pH	0.88	1.32
Temperature	70℃	70℃
Radius of particle	5 nm	5 nm
Ceramic species concentration	1 mM	8.8 mM
Electrolyte concentration	1×10^{-7}M	1×10^{-7}M

The interaction energies V_e, V_a, V_r and V_{tot} for each deposition setting can be calculated based on the equations and the parameters listed above. Typical curves for the V_e, V_a, V_r and V_{tot} for the deposition of ZrO_2 on SAM-coated silicon substrates is shown in Fig. 8.

For each of the four cases (ZrO_2 on SAM; ZrO_2 on bare Si; TiO_2 on SAM; TiO_2 on bare Si) in this study, there is a minimum of total interaction energy at the separation near 0.3 nm, while no repulsive energy barrier exists in the range of 0.3 nm to infinite. The electrostatic interaction is repulsive in that both the substrate and particle are positively charged in the relevant pH conditions; however, the magnitude of the electrostatic interaction is minimal, comparing with the attractive van der Waals interaction and the repulsive hydration interaction. The most significant force at distance > 0.2 nm is the van der Waals force, while at distance <0.2 nm the hydration force. The total interaction becomes negligible at separation larger than 5 nm, which is much smaller than the estimated average separation (>100 nm) between the oxide particles of 10 nm in size in the relevant deposition conditions. However, considering that the particles are actually in motion instead of static, it is possible that at some moment two particles would come close enough to be attracted to the equilibrium separation (0.3 nm). The Hamaker constants and the minimal interaction energies for substrate-solution-particle system (V_{ps}), for film-solution-particle system (V_{pf}), and for particle-solution-particle system (V_{pp}) are calculated and listed in Table 3.

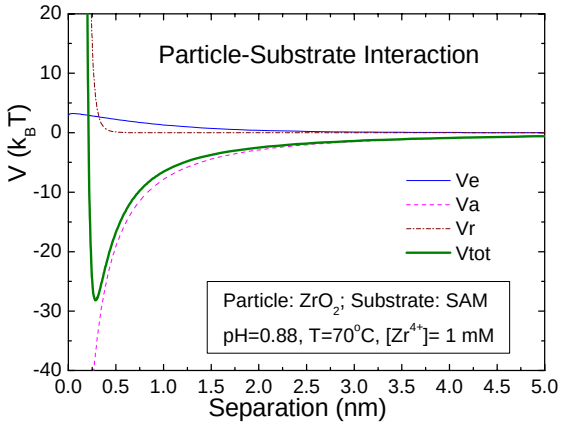

Fig. 8 Typical curves for particle-substrate interaction energies. A minimum of the total interaction energy (V_{tot}) occurs at the separation of around 0.3 nm.

Table 3 Calculated values of minimal interaction energies for particle-substrate (V_{ps}), particle-deposited film (V_{pf}), and particle-particle (V_{pp}) for different particle-substrate combinations.

	ZrO_2/SAM	**ZrO_2/Si**	**TiO_2/SAM**	**TiO_2/Si**
V_{ps}/k_BT	-28.17	-7.70	-39.69	-10.65
V_{pf}/k_BT	-54.18	-54.18	-107.76	-107.76
V_{pp}/k_BT	-30.67	-30.67	-60.78	-60.78

As revealed in Table 3, for the deposition of ZrO_2 and TiO_2 films on SAM or bare silicon, there is always a negative V_{ps} at separation of around 0.3 nm, indicating that the attraction between ceramic particles and the substrates (SAM coated or non-coated) is always thermodynamically favorable. On the other hand, the amplitudes of the V_{ps} for particle-SAM are larger than those for particle-bare silicon by a factor of about 4, implying that deposition of the oxide particles on SAMs has a much larger thermodynamic driving force than the deposition on bare silicon. The V_{pf} for the four cases are all negative, and their amplitude are larger than the corresponding V_{ps}, suggesting that the deposition would continue with a higher rate after a few monolayers of the ceramic materials are formed on the surface of substrates, which is consistent with the observation as discussed in Section 3. The lager amplitudes of V_{pf} than those of V_{pp} indicate that the oxide particles have larger tendency to continuously deposit on the substrates than to aggregate each other, after neglecting other factors such as particle separations and mass transport which may affect the actual deposition/aggregation process.

5. MECHANICAL PROPERTIES OF FILMS

In our previous study (Zhang et al., 2005), we proposed a method to measure the intrinsic modulus and the thickness of the ceramic thin films by using dynamic nanoindentations. By using this method, we have determined the average intrinsic moduli of the as-deposited ZrO_2 and the TiO_2 films to be 15.7± 4.5 GPa and 19.6±1.6 GPa, respectively. We also found that the film with finer particulate (i.e., clustered nanoparticles) structure exhibited higher intrinsic modulus than did that with coarser structure.

6. HERMETICITY OF CERAMIC FILMS

In order to implement the dye test for hermeticity of the coatings, polymer thin films, specifically parylene (poly-paraxylene) films were first conformally coated on every surface of the silicon substrates using a vapor phase deposition system (PDS 2010, Specialty Coating System, Indianapolis, IN). Thickness of the parylene films was controlled to be ≈ 1 μm. The parylene coatings were then cleaned and hydrolyzed by O_2 plasma in order to obtain a hydrophilic surface. The parylene coated silicon substrates were then deposited with SAMs and ceramic thin films with the same procedures as described in Section 2.

The as-deposited ZrO_2/SAM/parylene and TiO_2/SAM/parylene multilayer structures were immersed into a solution of fluorescent dye (Zyglo dye, V.O. Baker Co., Mentor, Ohio) for 48 h followed by rinsing with ethanol for complete removal of the dye from the surface. The parylene coatings together with the SAMs and ceramic films were then peeled off using Scotch tape. The remaining silicon substrates were inspected with a 4X microscope under the illumination of a UV light with wavelength of 365 nm. A typical intensity of the UV light at 38 cm from the bulb was 4300 mW/cm^2. Residues of the Zyglo dye, if there are any, would be activated by the UV light and easily discerned under the microscope. By counting the number of residue spots of the dye on the silicon substrate, we would be able to evaluate the hermetic property of the ceramic coatings, as compared to that of the polymer-only coating.

Our preliminary results showed that there were much less spots of the residue dye on the substrates coated with ZrO_2/SAM/parylene and TiO_2/SAM/parylene than those with only bare parylene, indicating that both the ZrO_2 and TiO_2 films enhanced the hermeticity performance of the parylene coatings. Specifically, the TiO_2 films claimed a much more significant enhancing effect.

CONCLUSIONS

Nanostructured ZrO_2 and TiO_2 thin films were deposited on silicon substrates by the hydrolysis of $Zr(SO_4)_2$ and $TiCl_4$ aqueous precursor solutions, respectively, at very low temperature (70°C) with the aid of SAMs terminated with phosphonate functionality. This deposition approach was inspired by the natural biomineralization process through which inorganic materials were deposited on a functionalized organic matrix in a controllable way. The as-deposited films consisted of nanocrystallites of tetragonal ZrO_2 and anatase phase TiO_2 in size of 5-10 nm, which displayed

virtually a random orientation at the film-substrate interfaces. Small amount of sulfur was found in the as-deposited ZrO_2 film, indicating the existence of amorphous phase of $Zr(SO_4)_2$; however, no chlorine was found in the as-deposited TiO_2 films. The principal mechanism for the nucleation of the films seems to be homogeneous nucleation. Unlike some previous results in this area, we found that the ZrO_2 and TiO_2 films can also be deposited on bare silicon substrates without any SAM coatings, provided that the right deposition conditions are employed. The deposition rate for the depositions on bare silicon is lower than that for those on SAMs in the initial stage, specifically in the initial 4 h; however, in the subsequent stages, the two exhibited similar deposition rate and finally yielded similar nanostructures and morphologies.

The DLVO theory was applied in this study to shed light on the mechanisms for the formation of the oxide films on SAMs in the media of aqueous precursor solutions. Despite many limits to the precise determination of the interaction energies, we found that for the 4 cases of depositions of ZrO_2 and TiO_2 on SAMs and bare silicon, negative minimum energies were always shown at around 0.3 nm for the interactions of particle-substrate, particle-deposited film, and particle-particle. It indicates that the initial and subsequent continuous deposition on both SAM and bare silicon as well as particle aggregation are all thermodynamically favorable. However, the differences in the magnitudes of minimum interaction energies may disclose some preference of the deposition on SAMs over that on bare silicon.

The intrinsic elastic moduli of the as-deposited ZrO_2 and TiO_2 films were determined to be 15.7± 4.5 GPa and 19.6±1.6 GPa, respectively. The ceramic films with finer structure exhibited higher intrinsic modulus than did those with coarser structure. It suggests a potential for further enhancement of mechanical properties by tailoring the microstructures. Dye leak tests suggest that the ZrO_2 and TiO_2 films, especially the latter one, can enhance significantly the hermeticity performance of the device coatings, making them excellent candidates for hermetic packaging.

ACKNOWLEDGMENTS

This research was sponsored by the Semiconductor Research Corporation (SRC) under contract number SRC 2003-TJ-1068 (monitored by Dr. H. Hosack). The TEM and SEM research in this paper was sponsored by the Assistant Secretary for Energy Efficiency and Renewal Energy, Office of FreedomCAR and Vehicle Technologies, as part of the High Temperature Materials Laboratory User Program, Oak Ridge National Laboratory, managed by UT-Battelle, LLC, for the U.S. Department of Energy under contract number DE-AC05-00OR22725. GZ and JC would also like to thank E. Boyle and T. Kanazawa at JEOL USA, Inc. for helping with the high-resolution TEM and SEM work on some of the ZrO_2 films.

REFERENCES

Ackler, H. D., Y. M. Chiang, et al. (1996). Comparisons of Hamaker constants for ceramic systems with intervening vacuum or water: From force laws and physical properties. *J. Colloid and Interface Sci.* **179**, 460.

Agarwal, M., M. R. De Guire, et al. (1997). Synthesis of ZrO2 and Y2O3-doped ZrO2 thin films using self-assembled monolayers. *J. Am. Ceram. Soc.* **80***,* 2967-2981.

Aizenberg, J., A. J. Black, et al. (1999). Control of crystal nucleation by patterned self-assembled monolayers. *Nature*, **398**, 495-498.

Gao, Y. F. and K. Koumoto (2005). Bioinspired ceramic thin film processing: Present status and future perspectives. *Crystal Growth & Design*, **5**, 1983-2017.

Hogg, R., T. W. Healy, et al. (1966). Mutual coagulation of colloidal dispersions. *Trans. Faraday Soc*., **62**,1638.

Israelachvili, J. N. (1985). Intermolecular and Surface Forces: With Applications to Colloidal and Biological Systems, Academic Press.

Kallay, N., E. Barouch, et al. (1987). Diffusional detachment of colloidal particles from solid/solution interfaces. *Advances in Colloid and Interface Science*, **27**, 1.

Maluf, N. (2000). An Introduction to Microelectromechanical Systems. Norwood, MA., Artech House, Inc.

Mann, S. (2001). Biomineralization: Principles and Concepts in Bioinorganic Materials Chemistry. New York, Oxford University Press, Inc.

Niesen, T. P. and M. R. De Guire (2001). Review: Deposition of ceramic thin films at low temperatures from aqueous solutions. *J. Electroceramics*, **6**, 169-207.

Rajan, N., C. A. Zorman, et al. (1998). Performance of 3C-SiC thin films as protective coatings for silicon-micromachined atomizers. *Thin Solid Films*, 315, 170-178.

Schmid, G. and L. F. Chi (1998). Metal clusters and colloids. *Adv. Mater.*, **10**, 515-526.

Shin, H., M. Agarwal, et al. (1998). Deposition mechanism of oxide thin films on self-assembled organic monolayers. *Acta Materialia,* **46**, 801-815.

Shin, H., R. J. Collins, et al. (1995). Synthesis and characterization of TiO_2 thin films on organic self-assembled monolayers. *J. Mater. Res.*, **10**, 692-698.

Yang, Q., G. Zhang, et al. (2004). Mechanical Behavior of Ceramic/SAM Bilayer. *Mater. Res. Soc. Symp. Proc.*, **844**,Y9.9.1

Zhang, G., D. A. Blom, et al. (2005). Nanostructured Ceramic Film Formation on Self-Assembled Monolayers via a Biomimetic Approach. *Mater. Res. Soc. Symp. Proc.*, **901E**, 0901-Ra21-06.1

Zhang, G., J. Y. Howe, et al. (2006). A biomimetic approach to the deposition of ZrO2 films on self-assembled nanoscale templates. *Mater. Sci. Eng. C*, **26**, 1344-1350.